

Testing Theoretical Models for the Higher-Order Moments of Dark Halo Distribution

R. Casas-Miranda, H.J. Mo and G. Boerner

Max-Planck-Institut für Astrophysik, Garching, Germany

ABSTRACT

Using high-resolution N-body simulations, we test two theoretical models, based either on spherical or on ellipsoidal collapse model, for the higher-order moments of the dark matter halo distribution in CDM models. We find that a theoretical model based on spherical collapse describes accurately the simulated counts-in-cells moments for haloes of several mass ranges. It appears that the model using ellipsoidal collapse instead of spherical collapse in defining dark haloes is unable to improve the models for the higher-order moments of halo distribution, for haloes much smaller than M^* (the mass scale on which the fluctuation of the density field has a rms about 1). Both models are particularly accurate for the descendants of haloes selected at high redshift, and so are quite useful in interpreting the high-order moments of galaxies. As an application we use the theoretical model to predict the higher-order moments of the Lyman break galaxies observed at $z \approx 3$ and their descendants at lower redshifts.

Key words: Galaxies: formation – galaxies: clustering – galaxies: haloes – cosmology: theory – dark matter

1 INTRODUCTION

In the standard scenario of galaxy formation, it is assumed that galaxies form by the cooling and condensation of gas within dark haloes (e.g. White & Rees 1978; White & Frenk 1991). The problem of galaxy clustering in space can then be approached by understanding the spatial distribution of dark haloes and galaxy formation in individual dark haloes. This approach is very useful for the following two reasons: (i) the formation and clustering properties of dark haloes can be modelled relatively reliably because of the simple physics involved (gravity only), (ii) realistic models of galaxy formation in dark haloes can now be constructed using either semi-analytic models (e.g. Kauffmann et al. 1999; Cole et al. 2000; Somerville & Primack 1999) or hydrodynamical simulations (e.g. Benson et al. 2001). Indeed, attempts have been made to use theoretical models of halo clustering to understand clustering properties of galaxies (e.g. Mo et al. 1997; Jing et al. 1998; Ma & Fry 2000; Scoccimarro et al. 2001; Peacock & Smith 2000; Seljak 2000). Most of these investigations use the theoretical models presented in Mo & White (1996) and in Mo et al. (1997) (hereafter MJW) to calculate the second-order and higher-order correlations of dark haloes. These models are based on the Press-Schechter formalism (Press & Schechter 1974) and its extensions (Lacey & Cole 1994).

The model prediction for the second moment, or the two-point correlation function, has been tested quite extensively by numerical simulations (Mo & White 1996; Mo et al.

1996; Jing 1998; Sheth & Tormen 1999; Governato et al. 1999; Colberg et al. 2000). The results show that the model proposed by Mo & White works reasonably well over a large range of halo masses. However, significant discrepancy between model and simulations results was found for low-mass haloes (Jing 1998; Sheth & Tormen 1999). Sheth et al. (2001) (hereafter SMT) suggested that the discrepancy at the low-mass end may be due to the fact that the model considered by Mo and White assumes spherical collapse for the halo formation while the collapse in a realistic cosmological density field may be better approximated by an ellipsoidal model. Indeed, SMT found that, if an ellipsoidal model is used, better agreement between the model and simulations results can be achieved in both the halo mass function and the two-point correlation function for low-mass haloes.

The performance of the MJW model for the higher-order moments of the halo distribution has been tested in their original paper using scale-free N-body simulations with relatively low resolution. Although their results show that the theoretical model matches the simulations results, the limited dynamical range in the simulations used by them does not allow one to test the model for a large range of halo masses. Furthermore, although the MJW model has been extended to include ellipsoidal dynamics (Sheth et al. 2001), this extension has not yet been tested by simulations results.

In this paper we use two sets of high-resolution simulations to test the MJW model and its extension. One set has a very large simulation box (and thus low mass resolu-

tion) which is used to control the finite-volume effect usually found in the analysis of higher-order moments of the galaxy distribution (Colombi et al. 1994). The other set has smaller simulation boxes but much higher mass resolutions which allows us to test the models for low-mass haloes.

The paper is organized as follows: The procedure to obtain the high order moments from counts-in-Cells is presented in section 2 along with theoretical models of these moments for dark haloes. Analysis of the simulations data and the comparison of the theory with the simulations results are presented in section 3. An application of the theoretical models to the higher-order moments of the Lyman-break galaxies (LBGs) is done in section 4. Because LBGs are highly biased (Adelberger et al. 1998), the skewness and kurtosis coefficients (S_3 and s_4) of LBGs and their descendants are significantly lower than those of the mass.

Finally, section 5 contains a summary of our results.

2 HIGHER-ORDER MOMENTS OF COUNTS-IN-CELLS

2.1 Definitions

The calculation of the counts-in-cells moments of a particle distribution and the relation of such moments to the corresponding moments of the underlying continuous density field are described in detail in Peebles (1980). We summarize the relevant formulae in the following.

The j^{th} central moment of counts in cells (we will use spherical cells whose radius will be denoted by R) of a point distribution is defined as

$$m_j(R) = \frac{1}{M} \sum_{i=1}^M (N_i - \bar{N})^j, \quad (1)$$

where N_i is the number of particles counted in the i^{th} sphere (cell), \bar{N} is the mean number of counts: $\bar{N}(R) = \frac{1}{M} \sum_{i=1}^M N_i(R)$, and the summation is over the M sampling spheres. Notice that \bar{N} is obtained directly from the counts.

The connected moments, μ_i , are defined through the central moments as

$$\mu_2 = m_2, \quad (2)$$

$$\mu_3 = m_3, \quad (3)$$

$$\mu_4 = m_4 - 3m_2^2. \quad (4)$$

These relations are written up to the 4th order because to this order they are relevant to our subsequent discussion. For a point process, the shot noise also contributes to the quantities μ_j . These contributions become significant for small radius where the mean count \bar{N} is small and should be properly subtracted. If the particle distribution is a Poisson sampling of the underlying density distribution, we can make the following subtractions to get the corrected connected moments:

$$k_2 = \mu_2 - \bar{N}, \quad (5)$$

$$k_3 = \mu_3 - 3\mu_2 + 2\bar{N}, \quad (6)$$

$$k_4 = \mu_4 - 6\mu_3 + 11\mu_2 - 6\bar{N}. \quad (7)$$

These quantities are related to the volume-averaged correlation functions by

$$\bar{N}^j \bar{\xi}_j = k_j, \quad (8)$$

where

$$\bar{\xi}_j = V_W^{-j} \int dr_1 \dots dr_j W(r_1) \dots W(r_j) \xi_j(r_1, \dots, r_j), \quad (9)$$

and $W(r)$ is a top-hat spherical window with volume V_W .

2.2 Theoretical Model for the Higher-Order Moments of Dark Halos

Mo et al. (1997) (MJW) have developed an analytical model for the hierarchical correlation amplitudes $[S_{j,h}(R) = \bar{\xi}_{j,h}/\bar{\xi}_{2,h}^{j-1}]$ for $j = 3, 4, 5$ in the quasi-linear regime, where the subscript h stands for quantities of dark haloes. In this model the statistical distribution of dark haloes within the initial density field, which is assumed to be Gaussian, is determined by an extension of the Press-Schechter formalism and the modifications of the distribution due to gravitationally induced motions are treated by means of a spherical collapse model (Mo & White 1996). The main results from this model, which are relevant for our analysis, are summarized as follows.

For the skewness and kurtosis ($j = 3, 4$), following the same notation as in MJW, one has:

$$S_{3,h} = b^{-1}(S_3 + 3c_2), \quad (10)$$

$$S_{4,h} = b^{-2}(S_4 + 12c_2S_3 + 4c_3 + 12c_2^2), \quad (11)$$

where S_3 and S_4 are the skewness and kurtosis of the underlying mass density field, $c_k = b_k/b$, $b = b_1$, and the constants b_k are the coefficients in the expansion of the bias relation:

$$\delta_h = \sum_{k=0}^{\infty} \frac{b_k}{k!} \delta^k, \quad (12)$$

where δ_h is the overdensity of haloes smoothed in a given window and δ is the corresponding overdensity of mass. The coefficients b_k for a halo with mass M_1 corresponding to a linear overdensity δ_1 , which collapses at redshift $z_1 = \delta_1/\delta_c - 1$ (with the critical overdensity for spherical collapse being $\delta_c = 1.686$), are given by:

$$b_1 = 1 + \frac{\nu_1^2 - 1}{\delta_1}, \quad (13)$$

$$b_2 = 2(1 + a_2) \frac{\nu_1^2 - 1}{\delta_1} + \left(\frac{\nu_1}{\delta_1} \right)^2 (\nu_1^2 - 3), \quad (14)$$

$$b_3 = 6(a_2 + a_3) \frac{\nu_1^2 - 1}{\delta_1} + 3(1 + 2a_2) \left(\frac{\nu_1}{\delta_1} \right)^2 (\nu_1^2 - 3) + \left(\frac{\nu_1}{\delta_1} \right)^2 \frac{\nu_1^4 - 6\nu_1^2 + 3}{\delta_1}, \quad (15)$$

where $\nu_1 \equiv \delta_1/\sigma(M_1)$ [with $\sigma(M_1)$ being the rms of the density fluctuation given by the density spectrum linearly extrapolated to the present time], $a_2 = -\frac{17}{21}$ and $a_3 = \frac{341}{567}$ are coefficients in the expansion of $\delta_0(\delta)$, the relation between the real mass overdensity δ and the corresponding quantity

obtained using linear theory (see equation A4 in MJW). The above bias coefficients are for the present-day descendants (at redshift $z_0 = 0$) of haloes identified at redshift z_1 . It can be easily extended to the case where $z_1 > z_0 > 0$. In this case, we replace δ_1 by $\delta_1 D(z_0)/D(0)$ (where $D(z)$ is the linear growth rate evaluated at redshift z) while keeping ν_1 unchanged.

If an ellipsoidal model is used to define collapsed haloes, the coefficients b_k take the following forms (Scoccimarro et al. 2001):

$$b_1 = 1 + \epsilon_1 + E_1, \quad (16)$$

$$b_2 = 2(1 + a_2)(\epsilon_1 + E_1) + \epsilon_2 + E_2, \quad (17)$$

$$b_3 = 6(a_2 + a_3)(\epsilon_1 + E_1) + 3(1 + 2a_2)(\epsilon_2 + E_2) + \epsilon_3 + E_3, \quad (18)$$

where

$$\epsilon_1 = \frac{\alpha\nu^2 - 1}{\delta_1},$$

$$\epsilon_2 = \frac{\alpha\nu^2}{\delta_1^2}(\alpha\nu^2 - 3), \quad (19)$$

$$\epsilon_3 = \frac{\alpha\nu^2}{\delta_1^3}(\alpha^2\nu^4 - 6\alpha\nu^2 + 3), \quad (20)$$

$$E_1 = \frac{2p/\delta_1}{1 + (\alpha\nu^2)^p},$$

$$\frac{E_2}{E_1} = \frac{1 + 2p}{\delta_1} + 2\epsilon_1, \quad (21)$$

$$\frac{E_3}{E_1} = 4(p^2 - 1) + \frac{6p\alpha\nu^2}{\delta_1^2} + 3\epsilon_1^2, \quad (22)$$

$$(23)$$

and $\alpha = 0.707$, $p = 0.3$. These formulae reduce to the original MJW model for $\alpha = 1$ and $p = 0$.

Inserting the expressions for b_k in equations (10) and (11) and taking S_3 and S_4 in these equations as the skewness and kurtosis of the mass distribution measured directly from the N-Body simulations, we can calculate the skewness and kurtosis for the distribution of dark haloes as predicted by the MJW model and its SMT extension (i.e. the model with ellipsoidal collapse).

3 SKEWNESS AND KURTOSIS OF DARK HALOES IN N-BODY SIMULATIONS

3.1 Simulations

In the present analysis we use two sets of cosmological N-body simulations, which have been obtained as part of the VIRGO (Jenkins et al. 1998) and the GIF (Kauffmann et al. 1999) projects. These two sets of simulations differ in the size of the simulation boxes and in the mass resolution, with the VIRGO simulations having larger simulation boxes and lower mass resolutions than the GIF ones. From the VIRGO simulations we have analyzed the Λ CDM model in order to test the MJW model in a volume large enough so that the effects due to the finite sampling volume may be negligible

(see below). We compare the results with those obtained from the GIF simulations to see how comparisons between models and simulations can be made for simulations with relatively small volume. For the GIF simulations, we focus on the τ CDM and Λ CDM models. The parameters characterizing the simulations are summarized in table 1. Further details can be found in Kauffmann et al. (1999) and Jenkins et al. (1998).

For each simulation there are several output files corresponding to different evolutionary times (redshifts) and for each of these output times there is a halo catalog containing information about haloes identified using the friends-of-friends group-finder algorithm with a linking length 0.2 times the mean interparticle separation. Only haloes containing 10 or more particles are included in the halo catalogues. In the case of the GIF simulations at redshift zero, which are used to compare the predictions of the models for haloes with low masses, unbound objects are excluded from the catalogues (see section 3.2 for details). The physical quantities available from each of these halo catalogues are: the index of the most-bound particle in the halo, which corresponds to the position of the halo as well as the central ‘galaxy’ within it; the virial radius (R_{vir}), defined as the radius (from the central particle) within which the overdensity of dark matter is 200 times the critical density; the virial mass (M_{vir}), which is the mass (or, equivalently, the total number) of dark matter particles within the virial radius; the circular velocity [$V_c = (GM_{vir}/R_{vir})^{1/2}$].

We have also generated several catalogues of the present-day positions of the central objects corresponding to the most-bound particles in haloes identified at an earlier epoch. This catalogues might be interpreted as ‘galaxy catalogues’ if we assume that the positions of galaxies at the present epoch correspond to those of the central particles within virialized objects identified at high redshifts. This concept is related to the assumption in models of galaxy formation that galaxies form by the cooling and condensation of gas within dark matter haloes (White & Frenk 1991). However, this interpretation does not take into account subsequent galaxy mergers.

We apply the counts-in-cells analysis described in the last section to the mass distributions and halo catalogues. To do this, we place spheres in a regular mesh of 30^3 centers and count the number of objects at each center over a set of concentric spheres which allows us to compute the desired statistical quantities at different radii.

3.2 Results

Following the procedure given in section 2.1 we have obtained the volume-averaged correlation functions up to the fourth order from the mass distribution and from the various halo samples. Analyses have been performed for two different cases. In the first, the higher-order moments are calculated at the same time when the dark haloes are identified. In the second, haloes are identified at some high redshift while the calculations of the higher-order moments are performed for their descendants at a later time. In all cases, the redshift at which halo identification is made is denoted by z_1 , while the redshift at which the higher-order moments are calculated is denoted by z_0 .

In Figures 1 and 2 we show the third- and fourth- order

Model	Ω_0	Ω_Λ	h	σ_8	Γ	Box Size [Mpc/h]	N_p	$m_p/h^{-1}M_\odot$
GIF- τ CDM	1.0	0.0	0.5	0.60	0.21	85	256^3	1.0×10^{10}
GIF- Λ CDM	0.3	0.7	0.7	0.90	0.21	141	256^3	1.4×10^{10}
VIRGO- Λ CDM	0.3	0.7	0.7	0.90	0.21	239.5	256^3	6.86×10^{10}

Table 1. Parameters characterizing the simulations used in the paper. Ω_0 and Ω_Λ are the density parameters for matter and for the cosmological constant, respectively, h is the Hubble parameter, σ_8 is the rms of the density field fluctuations in spheres of radius $8h^{-1}$ Mpc, and Γ is the shape parameter of the power spectrum. Also given are the size of the simulation box, the total number of particles and the mass per dark matter particle in a simulation.

moments from the VIRGO Λ CDM simulation, together with model predictions. For haloes identified and analyzed at a given epoch (Figure 1) both models work remarkably good for scales larger than r_0 [$\xi_2 = 1$], which are the validity scales of the models, and in particular for haloes with intermediate masses. Both models are less accurate for very low mass haloes and for very massive haloes. On the other hand, in the case of present epoch descendants of haloes identified at an earlier epoch, both models work remarkably good in the validity scales of the models, as shown in Figure 2.

In these two figures we also plot the prediction of the MJW model with S_3 and S_4 given by perturbation theory (see Bernardeau 1994). The fact that this prediction also matches the simulations results suggests that the moments obtained from the VIRGO simulations are not affected significantly by the finite-volume effect and that the MJW model is a good approximation to the higher-order moments for haloes that are not much smaller than M_* [defined by $\sigma(M_*) = 1.68$].

With their high mass resolutions, GIF simulations allow us to test the theoretical models for haloes with mass $M \ll M_*$. Since the GIF simulations have relatively small simulation boxes, the higher-order moments are expected to be affected significantly by the finite-volume effect (Colombi et al. 1994). However, this effect in each simulation is expected to be similar for both the mass distribution and the halo distribution. Thus, to test the bias model given in (10) and (11) by a numerical simulation we should use the value of S_3 and S_4 obtained directly from mass distribution in the simulations, because it is the simulated power spectrum (not the theoretical one) that is responsible for the clustering in the simulations. Figures 3 and 4 show the results obtained for the GIF simulations, along with the predictions from the models, for present epoch descendants of haloes identified at earlier epochs. It can be noticed that the predictions from both models, MJW and SMT, are in good agreement with the simulations results.

As we want to test and compare the performance of the models for low mass haloes at a given redshift, we have estimated the moments of counts-in-cells, as well as the moments predicted by the models, for several populations of sub- M_* haloes. It is well known that many of the low-mass haloes identified using a simple friends-of-friends halo finding algorithm have positive total energy (i.e., are unbound groups) and that these unbound haloes are expected to have a significant effect on higher-order statistics (Benson et al. 2001). For this reason we have revised our GIF halo catalogues for possible unbound haloes. The total energy for each halo in the catalog is computed, if it is positive the

least bound particle in the group is removed and the total energy is computed again. This process is repeated for each halo until the total energy becomes negative or until there are remaining less than 10 particles in the group. If the last condition is reached, the halo is removed from the catalog. We found that $\sim 10\%$ of the haloes in the original catalog have to be removed from it, in agreement with Benson et al. (2001).

Figures 5 and 6 show the results for present epoch haloes less massive than M_* in the revised GIF halo catalogues, along with the predictions from the models. For haloes with masses much smaller than M_* , the SMT extension overestimates the skewness and kurtosis, while the MJW model gives a better fit to the simulations results. Thus, although the SMT extension improves the models for the mass function and the second order model of dark haloes, it seems to be unable to improve the models for the higher-order moments. It is not clear why this happens, it might be a fluke or it might also mean that the simple model for the higher-order moments, either spherical or ellipsoidal, does not work accurately.

From a comparison between the VIRGO and GIF results, it is evident that both the skewness and kurtosis are strongly affected by the finite-volume effect. However, if the loss of clustering power due to the finite volume is taken into account, the model predictions are in good agreement with the numerical results, suggesting that the bias relations given by (10) and (11), with the coefficients given by the extended Press-Schechter formalism, are good approximations to the skewness and kurtosis of dark haloes in the quasi-linear regime.

To see more clearly the difference between the MJW model and the SMT extension, we show in Figure 7 the amplitudes of the halo skewness and kurtosis at a fixed radius ($R = 10h^{-1}$ Mpc) as a function of the linear bias parameter $b = b_1$ [see equations (13) and (16)]. The curves correspond to the predictions from the models for the present-day descendants of haloes at three values of z_1 (3.0, 1.0 and 0.0). From the figure we see that in all cases the values of $S_{j,h}$ are lower than those for the mass unless b is comparable to or smaller than 1. This result was obtained in MJW based on the spherical model. We see that this is also true even if the SMT extension is used, although the amplitudes of $S_{j,h}$ given by the elliptical model are higher than those given by the spherical model for a given b . These features in $S_{3,h}$ and $S_{4,h}$ have been used in MJW to constrain the bias parameter b for galaxies.

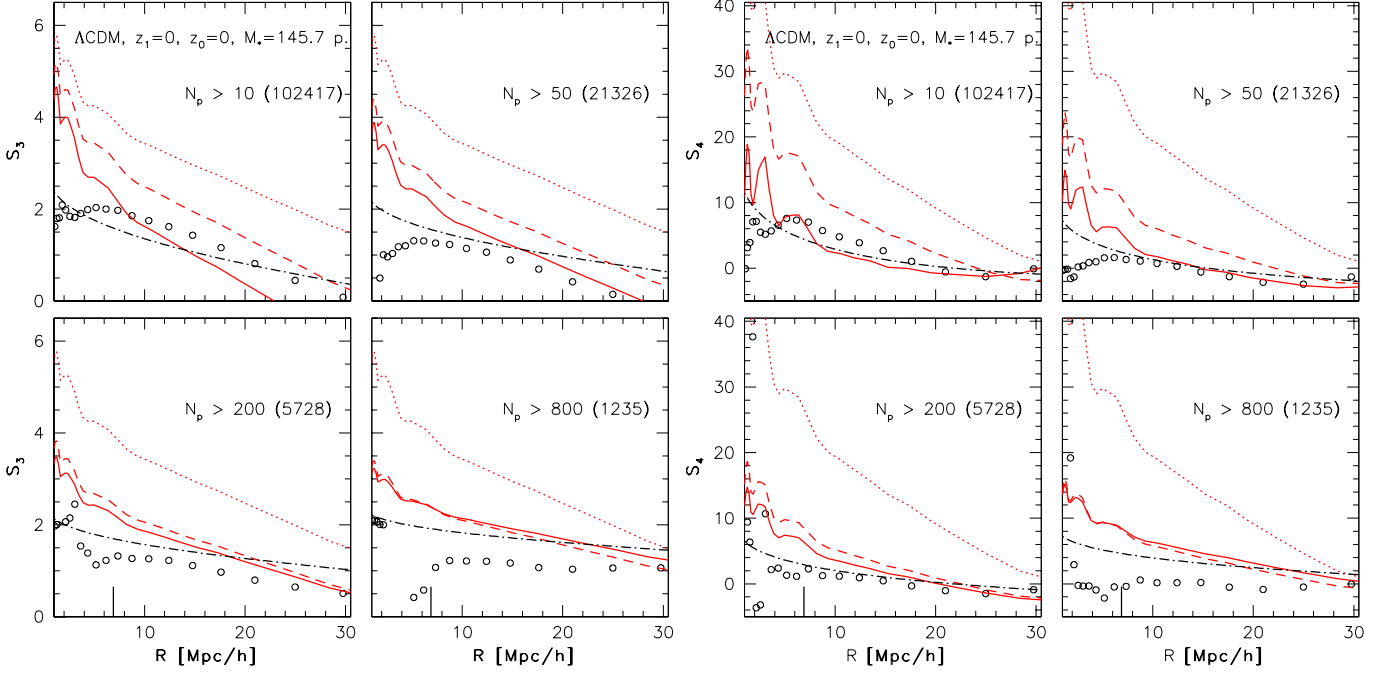


Figure 1. Skewness S_3 and kurtosis S_4 of dark haloes with different mass ranges obtained from counts-in-cells analysis (symbols), from applying the bias model from MJW (solid line) and its SMT extension (dashed-line). The moments for the mass distribution are shown by the dotted line and the moments for the haloes obtained using the moments for the mass from the perturbation theory are shown as a dot-long dashed line. The thick ticks on the horizontal axis show the scales where $\bar{\xi}_2(R) = 1$. Results are shown for the VIRGO Λ CDM simulations. The haloes have been identified and analyzed at the times written in the upper-left boxes. The value of M_* is also written for more information. Each box corresponds to a different range of masses of haloes, as appearing in the labels. The quantities between parenthesis correspond to the number of haloes in each sample.

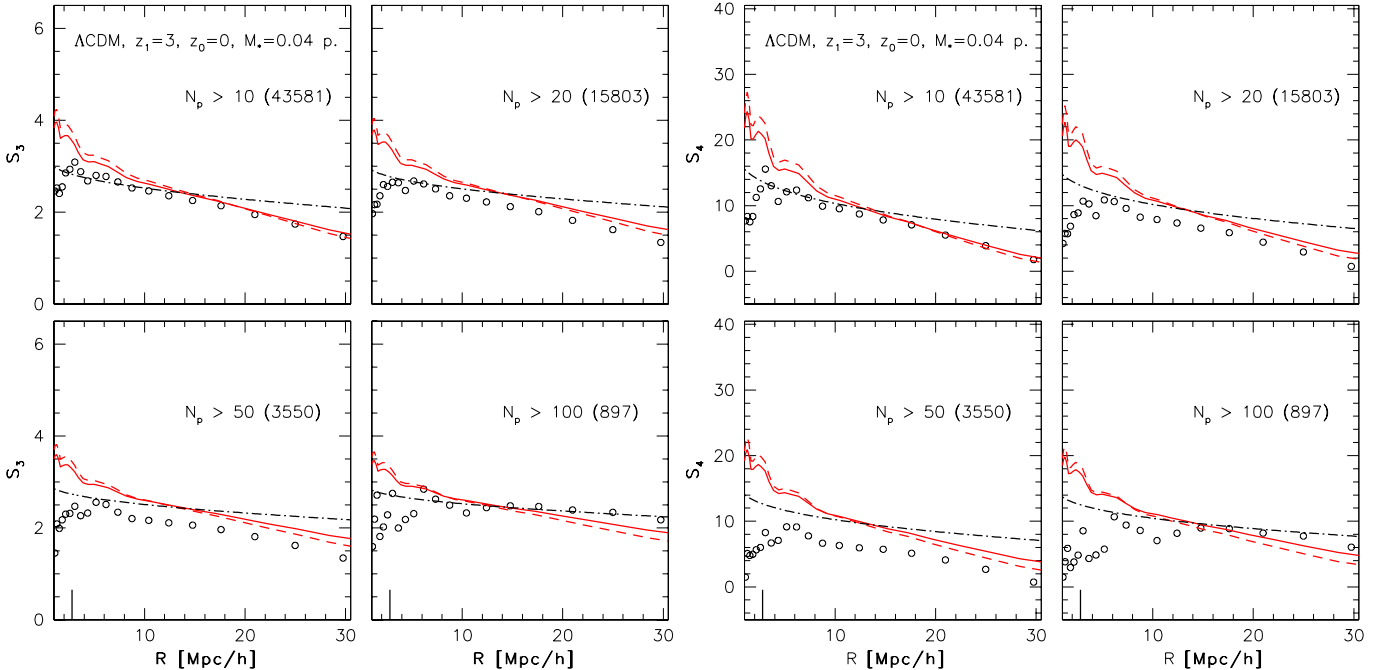


Figure 2. Skewness S_3 and kurtosis S_4 for haloes in the VIRGO Λ CDM simulations for haloes identified at $z = 3$ and analyzed at present time. The lines and symbols correspondence is the same as in Figure 1 as well as the notation.

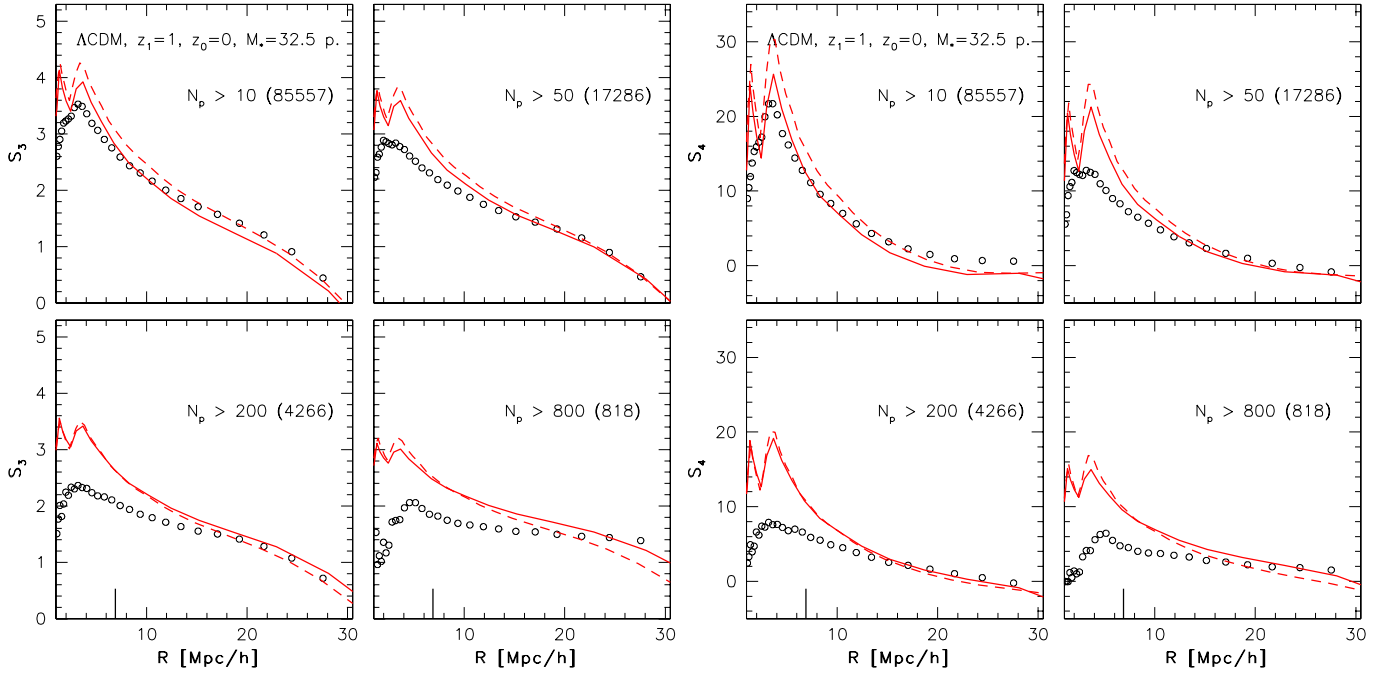


Figure 3. Skewness S_3 and Kurtosis S_4 of dark haloes with different mass ranges obtained from counts-in-cells analysis (symbols) and from applying the bias model from MJW (solid line) and its SMT extension (dashed-line). The thick ticks on the horizontal axis show the scales where $\xi_2(R) = 1$. Results are shown for the GIF Λ CDM model and for haloes identified at $z = 1$ and analyzed at the present time.

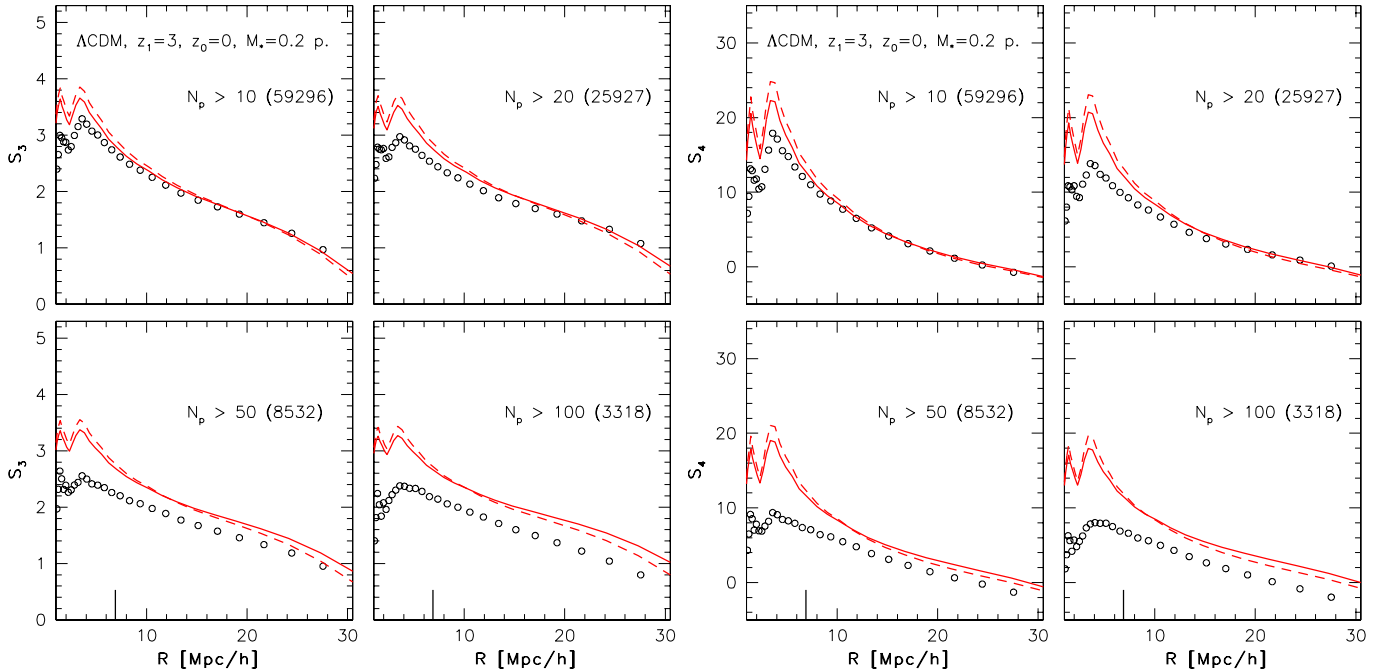


Figure 4. Skewness S_3 and Kurtosis S_4 of dark haloes with different mass ranges obtained from counts-in-cells analysis (symbols) and from applying the bias model from MJW (solid line) and its SMT extension (dashed-line). The thick ticks on the horizontal axis show the scales where $\xi_2(R) = 1$. Results are shown for the GIF Λ CDM model and for haloes identified at $z = 3$ and analyzed at the present time.

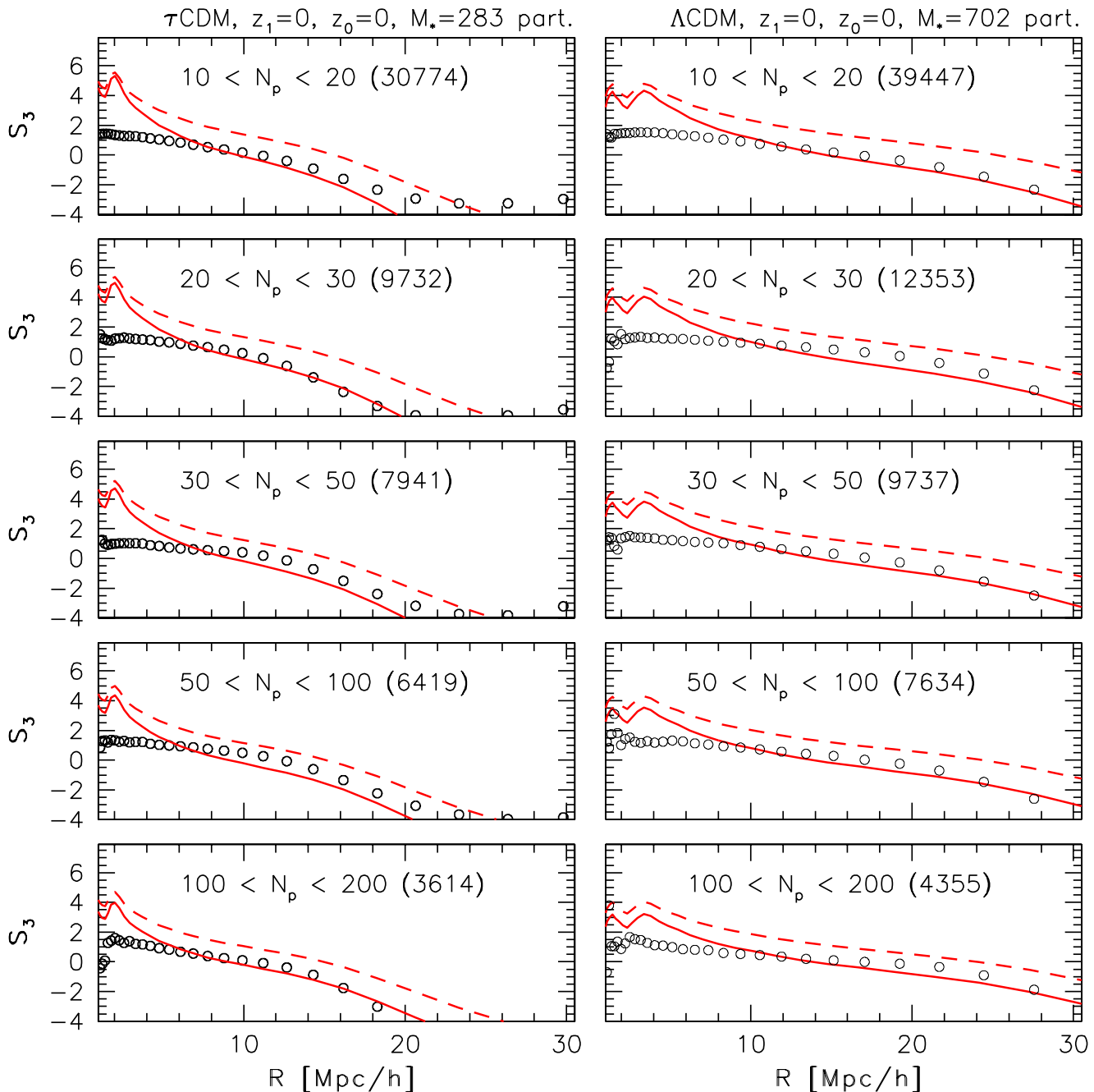


Figure 5. Skewness S_3 obtained from counts-in-cells analysis (symbols) and from applying the bias model from MJW (solid line) and its SMT extension (dashed-line) of haloes less massive than M_* . Each row in the panel corresponds to a different range of halo masses, as indicated in the boxes.

4 DISCUSSION

From the results shown in Figure 7 we see that for present time descendants of haloes already formed at a given redshift ($z > 0$), the values of the skewness and kurtosis depend only weakly on the object mass if the bias parameter b is larger than or near to one. On the other hand, in the same range of b it is clear that the high order moments depend on the identification redshift, which is associated with the redshift of formation of the objects, with the corresponding values increasing as the formation redshift increases. Therefore the

values of the skewness and kurtosis of old objects, like elliptical galaxies, are expected to be higher than the corresponding moments of more recently formed objects, such as spiral galaxies. This feature can be useful in studying different galaxy populations.

We have used the models to analyze the predicted values of the high order moments for high redshift objects, like the Lyman Break Galaxies (LBGs), which are commonly assumed to form in the center of the most massive haloes at redshift ~ 3 (Mo & Fukugita 1996; Adelberger et al. 1998; Jing & Suto 1998; Mo et al. 1999). Under this assumption

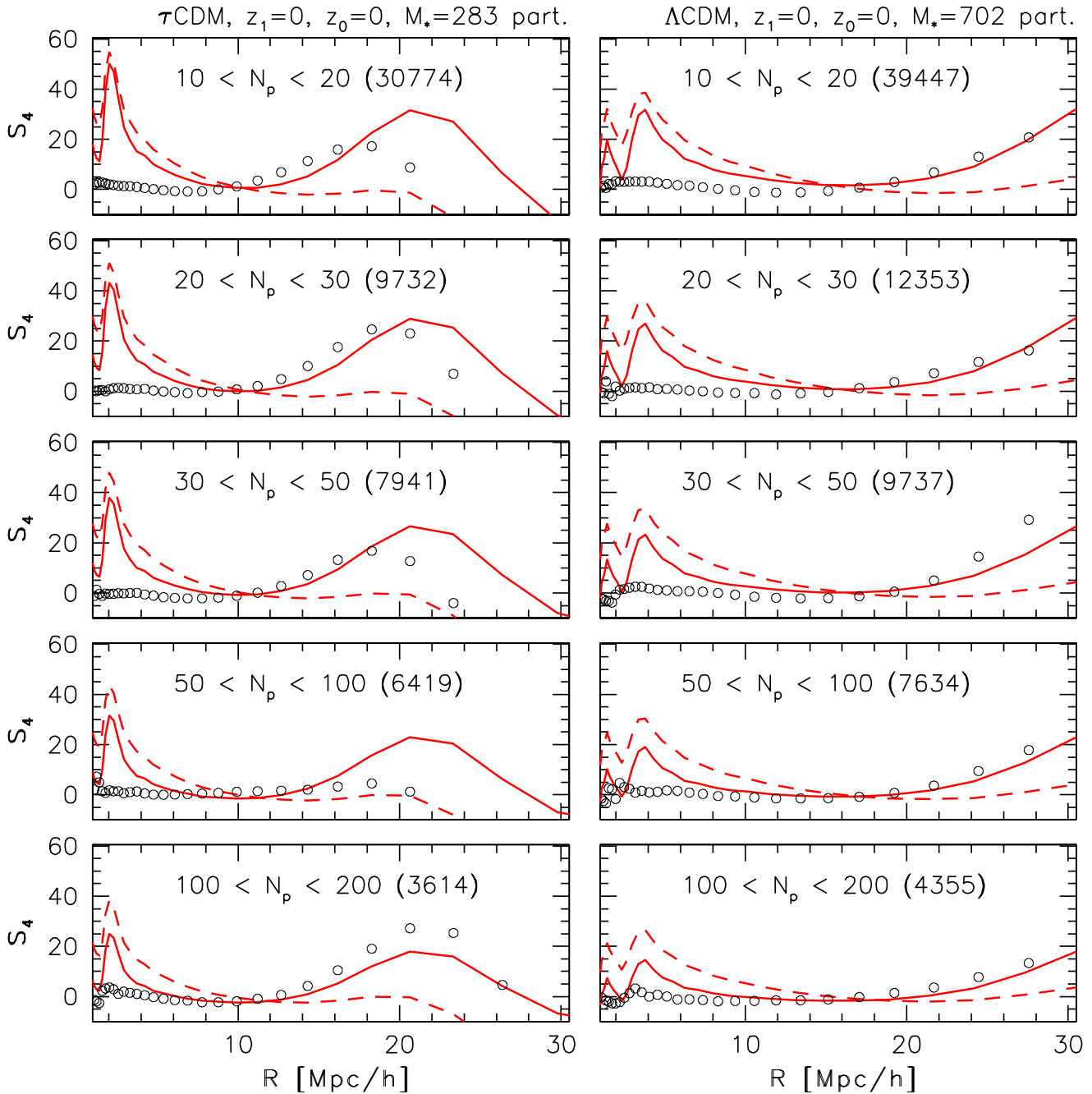


Figure 6. Kurtosis S_4 obtained from counts-in-cells analysis (symbols) and from applying the bias model from MJW (solid line) and its SMT extension (dashed-line) of haloes less massive than M_* . Each row in the panel corresponds to a different range of halo masses, as indicated in the boxes.

and supposing that only a negligible fraction of those haloes host a secondary observable galaxy the observed LBGs correspond to the most massive haloes at $z \sim 3$. We have estimated the predicted values for the skewness and kurtosis at a fixed scale $R = 10 h^{-1} \text{ Mpc}$ of the LBGs ($z = 3$) and their descendants at a given redshift z . We chose this value of R because the mass density in the universe is still in the quasi-linear regime and the high order moments of galaxy distributions are more difficult to measure on much larger scales.

For our estimates we have used the coefficients as given

by equations (13)-(15), where the S_q ($q = 3,4$) for the mass distribution are obtained from linear perturbation theory (Bernardeau 1994), and the weighted average needed to get the effective b_k 's is derived either by means of the mass function from the Press-Schechter formalism, for the predictions from the MJW model, or by means of the mass function predicted by the SMT model, for the predictions from the SMT model. The main parameter for the estimation of the b_k 's for the LBGs corresponds to the observed abundance of LBGs, namely the number density given by (Adelberger et al. 1998). This number is $N_{lbg} \approx 8 \times 10^{-3} h^3 \text{ Mpc}^{-3}$ at

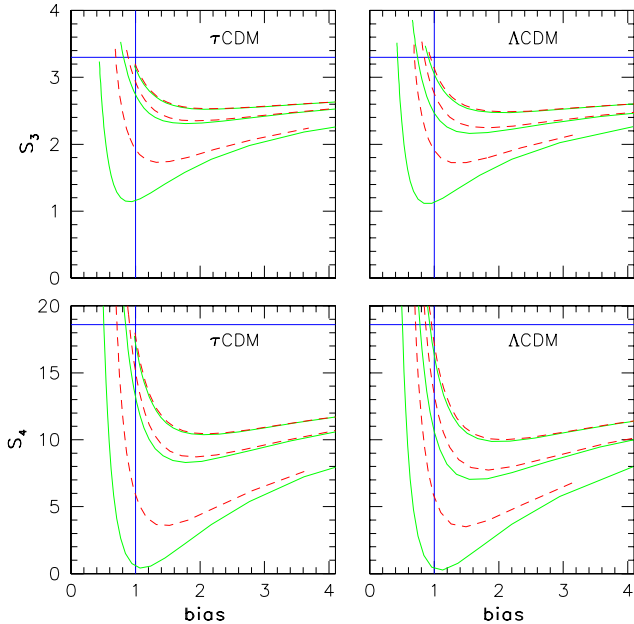


Figure 7. Predictions from the MJW model (solid lines) and its SMT extension (dashed-line) for the skewness and kurtosis of haloes at a radius $R = 10 h^{-1} Mpc$ as a function of the linear bias parameter b . each pair of curves shows the results for a given δ_1 , where $z_1 \equiv (\delta_1/1.686 - 1) = 0., 1.0, 3.0$) from bottom to top.

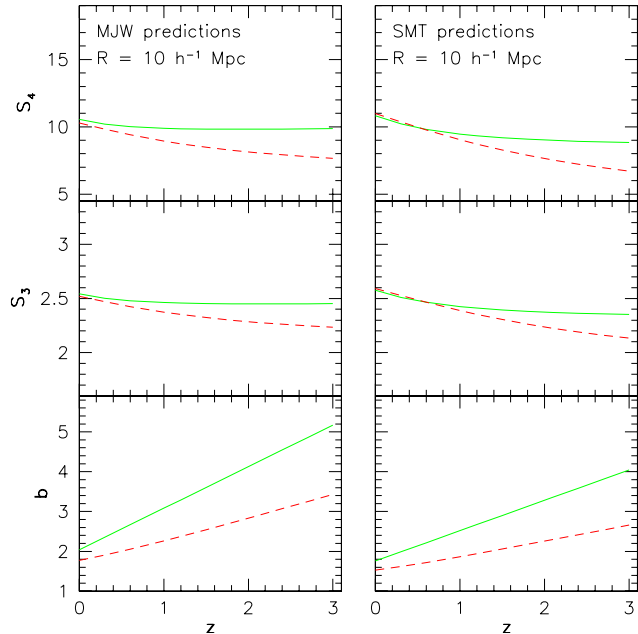


Figure 8. Skewness and kurtosis at $R = 10h^{-1} Mpc$ for the LBGs at $z = 3$ and their descendants at later epochs. The curves correspond to the Λ CDM model (dashed lines) and the τ CDM model (solid lines). The left panel shows the predictions from the MJW model and the right panel shows the predictions from the SMT extension.

$z \sim 3$ for an Einstein-de Sitter universe, and is similar to the present abundance of L_* galaxies. The corresponding number for the Λ CDM universe is estimated by multiplying this number by the comoving volume per unit redshift at $z \sim 3$ for an Einstein-de Sitter universe divided by the corresponding value for the Λ CDM universe.

In Figure 8 we show the values of the skewness, the kurtosis and the linear bias at $R = 10 h^{-1} Mpc$ of the LBGs, as a function of the redshift, in the Λ CDM and τ CDM models. From the curves we see that, although the linear bias parameter is quite different in both CDM models, the values obtained for the moments are quite similar and so these statistics do not provide stringent constraints on cosmological parameters. Note that because LBGs are highly biased relative to the mass (Adelberger et al. 1998), the skewness and kurtosis parameters of their haloes and descendants are significantly lower than those for the mass. Thus, observations on these quantities may give additional evidence that these objects are highly biased.

Finally in Figure (9) we show the higher-order moments from the spatial distribution of model galaxies in the GIF Λ CDM simulations at redshifts ($z = 0, 1$ and 3), along with the corresponding quantities of the distribution of haloes hosting the galaxies and with the same quantities of the distribution of haloes weighted by the number of galaxies hosted by each halo. The catalogues are limited to model galaxies with stellar masses greater than $\sim 2 \times 10^{10} h^{-1} M_\odot$ (i.e., haloes more massive than $10^{12} h^{-1} M_\odot$). For further details about these catalogues and the galaxy formation models used in their construction see Kauffmann et al. (1999).

From the plots it can be seen that the skewness and kurtosis of model galaxies at redshift 1 and 3 is similar to the corresponding quantities of the dark matter halo population hosting the model galaxies ($M_h > 10^{12} h^{-1} M_\odot$). The difference between the moments of the model galaxies and dark matter haloes are still appreciable since there are haloes hosting more than one galaxy and this have strong effects on clustering quantities like the higher-order moments. Nevertheless, the similarities shown in the plots suggest that, indeed, one may assume that the distribution of galaxies may be approximated by the distribution of dark matter haloes. Indeed from the plot it can be seen that the moments of the distribution of model galaxies are very similar to the moments of the distribution of dark matter haloes weighted by the number of galaxies hosted by each halo. At small scales the moments of the weighted halo distribution are larger than the moments of the model galaxies distribution because we neglect any structure information in a halo containing several model galaxies.

Thus, one might be able to describe the higher-order moments of galaxies by combining the theoretical models for the higher-order moments of dark matter haloes with models for the number, stellar mass and position of individual galaxies that can be hosted by a single dark matter halo with mass M at a given epoch. Furthermore, many of the semi-analytic model galaxies at redshift 3 would be included in current LBGs samples and thus are close to a subset of the LBGs population, which is highly biased respect to the mass. From the figure we see that $S_3 \sim 2$ and $S_4 \sim 5$ at $R = 10 Mpc/h$, which is nearly consistent with the model predictions shown in Figure 8.

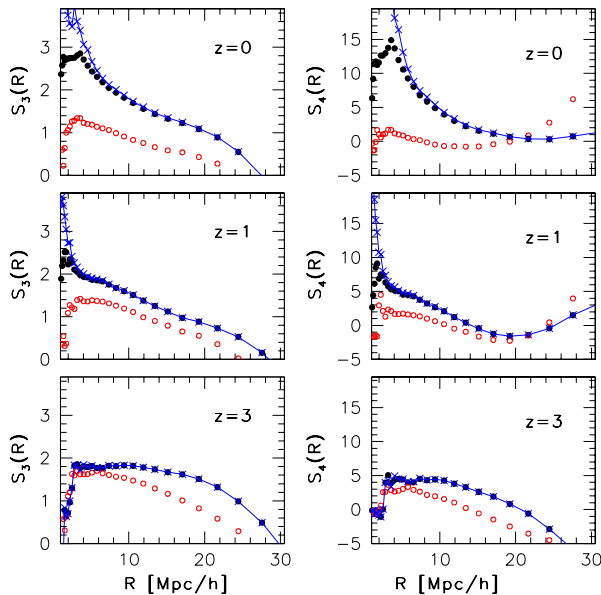


Figure 9. Skewness S_3 and kurtosis S_4 of the spatial distribution of galaxies obtained from the GIF Λ CDM simulations using semi-analytical models of galaxy formation (filled circles). S_3 and S_4 of the distribution of haloes hosting the galaxies is also plotted (open circles). For comparison, the respective quantities of the distribution of haloes weighted by the number of galaxies they host is included (crosses connected through a line).

5 SUMMARY

We have tested the MJW model and its SMT extension using two sets of high-resolution N-body simulations with different simulation boxes and mass resolution. From the set with the very large simulation box, which allows us to control the finite volume effect, we found that the models work remarkably good for CDM universes. The good performance of the models when the moments from the mass distribution are estimated using the linear perturbation theory, shows that the moments from this set (VIRGO) are practically unaffected by the finite volume effect. The other set of simulations, having much higher mass resolution, has been used to test the model for low-mass haloes, showing that the model based on spherical collapse (MJW) works better than the model based on ellipsoidal collapse (SMT) in describing the higher-order moments of haloes less massive than M^* . For massive haloes both models work remarkably good.

We use the theoretical models to predict the higher-order moments at a fixed scale of the Lyman break galaxies observed at $z = 3$ and their descendants at lower redshifts. We found that, although the linear bias parameter b depends strongly on the cosmology adopted, the values of the higher-order moments are practically the same in both CDM models and therefore the higher-order moments from the spatial distribution of these objects cannot be used to constrain cosmological parameters.

ACKNOWLEDGMENTS

We thank the GIF group and the VIRGO consortium for the public release of their N-body simulations data (www.mpa-garching.mpg.de/Virgo/data_download.html). R. Casas-Miranda acknowledges financial support from the “Francisco José de Caldas Institute for the Development of Science and Technology (COLCIENCIAS)” under its scholarships program. We thank our referee for useful comments and suggestions.

REFERENCES

- Adelberger K. L., Steidel C. C., Giavalisco M., Dickinson M. E., Pettini M., Kellog M., 1998, *ApJ*, 505, 18
 Benson A. J., Frenk C. S., Baugh C. M., Cole S., Lacey C. G., 2001, *MNRAS*, 327, 1041
 Bernardeau F., 1994, *ApJ*, 433, 1
 Colberg J. M., White S. D. M., Yoshida N., MacFarland T. J., Jenkins A., Frenk C. S., Pearce F. R., Evrard A. E., Couchman H. M. P., Efstathiou G., Peacock J. A., Thomas P. A., The Virgo Consortium 2000, *MNRAS*, 319, 209
 Cole S., Lacey C. G., Baugh C. M., Frenk C. S., 2000, *MNRAS*, 319, 168
 Colombi S., Bouchet F. R., Shaeffer R., 1994, *Astron. Astrophys.*, 281, 301
 Governato F., Babul A., Quinn T., Tozzi P., Baugh C. M., Katz N., Lake G., 1999, *MNRAS*, 307, 949
 Jenkins A., Frenk C. S., Pearce F. R., Thomas P. A., Colberg J. M., White S. D. M., Couchman H. M. P., Peacock J. A., Efstathiou G., Nelson A. H., 1998, *ApJ*, 499, 20
 Jing Y. P., 1998, *ApJL*, 503, L9
 Jing Y. P., Mo H. J., Boerner G., 1998, *ApJ*, 494, 1
 Jing Y. P., Suto Y., 1998, *ApJ*, 494, L5
 Kauffmann G., Colberg J. M., Diaferio A., White S. D. M., 1999, *MNRAS*, 303, 188
 Lacey C., Cole S., 1994, *MNRAS*, 271, 676
 Ma C. P., Fry J. N., 2000, *ApJ*, 531, 87
 Mo H., Jing Y. P., White S. D. M., 1997, *MNRAS*, 284, 189
 Mo H. J., Fukugita M., 1996, *ApJL*, 467, L9
 Mo H. J., Jing Y. P., Börner G., 1997, *MNRAS*, 286, 979
 Mo H. J., Jing Y. P., White S. D. M., 1996, *MNRAS*, 282, 1096
 Mo H. J., Mao S., White S. D. M., 1999, *MNRAS*, 304, 175
 Mo H. J., White S. D. M., 1996, *MNRAS*, 282, 347
 Peacock J. A., Smith R. E., 2000, *MNRAS*, 318, 1144
 Peebles P. J. E., 1980, *The Large-Scale Structure of the Universe*. Princeton Univ. Press
 Press W. H., Schechter P., 1974, *ApJ*, 187, 425
 Scoccimarro R., Sheth R. K., Hui L., Jain B., 2001, *ApJ*, 546, 20
 Seljak U., 2000, *MNRAS*, 318, 203
 Sheth R. K., Mo H. J., Tormen G., 2001, *MNRAS*, 323, 1+
 Sheth R. K., Tormen G., 1999, *MNRAS*, 308, 119
 Somerville R. S., Primack J. R., 1999, *MNRAS*, 310, 1087
 White S. D. M., Frenk C., 1991, *ApJ*, 379, 52
 White S. D. M., Rees M. J., 1978, *MNRAS*, 183, 341